Refined 1.89-Å Structure of the Histidine-Binding Protein Complexed with Histidine and Its Relationship with Many Other Active Transport/Chemosensory Proteins[†,‡]

Nanhua Yao,[§] Sergei Trakhanov,[§] and Florante A. Quiocho*[,§,∥]

Department of Biochemistry, Howard Hughes Medical Institute, and Department of Molecular Physiology and Biophysics, Baylor College of Medicine, Houston, Texas 77030

Received January 3, 1994; Revised Manuscript Received February 16, 1994[⊗]

ABSTRACT: The structure of the histidine-binding protein (HBP, M_r = 26 100), involved solely in active transport, has been determined by the molecular replacement technique and refined to 1.89-Å resolution and to an *R*-factor of 0.199. The structure is that of two protein molecules, each with a bound L-histidine, in the asymmetric unit. Replacement solution was achieved by using a model of the crystal structure of the ligand-free, open-cleft form of the lysine/arginine/ornithine-binding protein which was modified so that the two domains are close to each other by bending the hinge connecting the two domains. The bound histidine is held in place by 10 hydrogen bonds, 2 salt links, and about 60 van der Waals contacts. Elucidation of the HBP structure brings a total of eight different binding protein structures determined in our laboratory, including those with specificities for monosaccharides, maltodextrins (linear and cyclic), aliphatic amino acids, and inorganic oxyanions. These structures comprise about a third of the entire family of periplasmic binding proteins which act as initial primary high-affinity receptors of active transport in Gram-negative bacteria. Two of the binding proteins with specificities for glucose/galactose and maltodextrins also serve in a similar capacity in chemotaxis. Though these proteins have different molecular weights (ranging from 26 000 to 40 000), amino acid sequences, and ligand specificities, their three-dimensional structures are similar overall. They are elongated (axial ratios of 2:1) and composed of two similar globular domains separated by a deep cleft wherein the ligand-binding site is located. These structures provide understanding of molecular recognition of a variety of ligands at the atomic level and functional roles of the binding proteins.

The elucidation of the high-resolution three-dimensional structures of several members of a family of proteins, collectively called "binding proteins", found in the periplasmic space of Gram-negative bacteria has been the focus of our attention for some time. This has been driven mainly by our desire to obtain a high-resolution portrait of this protein family and to dissect the features of molecular recognition, at the atomic level, of a wide variety of ligands such as monosaccharides, linear and cyclic oligosaccharides, amino acids, dipeptides, and oxyanions. Producing crystals of eight different binding proteins that show diffraction to very high resolutions, between 1.9 and 1.2 Å, has provided a major impetus to our studies [for recent reviews, see Quiocho (1990, 1991)].

Binding proteins serve as initial high-affinity receptors of active transport systems or permeases [for reviews, see Furlong (1987) and Ames *et al.* (1986, 1990)]. These permeases further require heterooligomeric cytoplasmic membrane-bound proteins which are responsible for the actual ligand translocation and energy coupling (Furlong, 1987; Ames, 1990). Ames (1990) has summarized the genetic and biochemical evidence for the interaction between the periplasmic binding proteins and the membrane-bound transport components.

A handful of the binding proteins, including the glucose/galactose-binding protein and the maltodextrin-binding protein, are also involved in chemotaxis in a capacity similar to that in transport [for review, see MacNab (1987)]. Chemotaxis also requires membrane-associated components which are distinct from those of transport.

Binding proteins are not confined only to Gram-negative bacteria. Very recently, we have been able to show that the 38 000 extracellular antigen of the *Mycobacterium tuberculosis*, the strongest immunoreactive component of the bacteria, is a phosphate-binding protein with properties very similar to those of the *Escherichia coli* periplasmic phosphate-binding protein (Chang *et al.*, 1994). Sequence homology search has also implicated extracytoplasmic proteins in the Gram-positive *Streptococcus pneumoniae* and in *Mycoplasma hyorhinis* that bear considerable similarity with periplasmic binding proteins (Gilson *et al.*, 1988).

The histidine-binding protein (HBP),[1] along with the lysine/arginine/ornithine-binding protein (LAOBP), is one of the most extensively studied members of the binding protein family. This is due to a longstanding investigation by Ames and co-workers of these two basic amino acid-binding proteins from *Salmonella typhimurium* (Ames, 1986; Ames *et al.*, 1990). On the basis of the sequence of 238 amino acids, HBP from *S. typhimurium* has a molecular weight of about 26 100.

[†] This work was supported in part by grants from the NIH. N.Y. is a predoctoral fellow of the W. M. Keck Center for Computational Biology. F.A.Q. is an Investigator of the Howard Hughes Medical Institute.

[‡] Crystallographic coordinates have been deposited in the Brookhaven Protein Data Bank (reference number 1HSL).

* Author to whom correspondence should be addressed.

[§] Department of Biochemistry.

[∥] Howard Hughes Medical Institute and Department of Molecular Physiology and Biophysics.

[⊗] Abstract published in *Advance ACS Abstracts,* April 1, 1994.

[1] Abbreviations: HBP, histidine-binding protein; LAOBP, lysine/arginine/ornithine-binding protein; MBP, maltodextrin- or maltose-binding protein; rms, root mean square.

0006-2960/94/0433-4769$04.50/0

Both HBP and LAOBP contain an identical number of residues and about 70% sequence identity and interact with common membrane-bound components of active transport (Higgins & Ames, 1981; Higgins *et al.*, 1982; Ames, 1986). The same properties are found in both the leucine/isoleucine/valine-binding protein and the leucine-specific-binding protein (Nazos *et al.*, 1984; Landick & Oxender, 1985).

Equilibrium and rapid kinetic measurements of histidine binding to the *S. typhimurium* HBP showed tight binding and a fast association rate constant of histidine. These measurements gave K_d values of 0.64×10^{-7} M and 0.3×10^{-7} M, a k_{on} or association rate constant of 10 M^{-1} s^{-1}, and a k_{off} or dissociation rate constant of 9.7 s^{-1}, respectively (Miller *et al.*, 1983). These values are not greatly different from those obtained for the binding of the best substrates to four other binding proteins (Miller *et al.*, 1980, 1983).

Two groups have reported the crystallization of the histidine-binding protein; Kang *et al.* (1989) obtained crystals of *S. typhimurium* HBP that diffract up to 2.3-Å resolution on a rotating anode, and Trakhanov *et al.* (1989b) obtained crystals of the *E. coli* protein that diffract to 3-Å resolution. Here we report the acquisition of *E. coli* HBP crystals that surpass the quality of those reported previously and the determination and refinement of the HBP structure. (Note that hereafter, unless otherwise identified, HBP pertains to the *E. coli* protein.)

EXPERIMENTAL PROCEDURES

Protein Purification and Crystallization. The procedure for purifying HBP from *E. coli* K12 has been described previously (Trakhanov, 1989). The stock HBP solution, which is stored at 4 °C, is composed of 10 mg/mL protein, 0.5 mM L-histidine, and 10 mM sodium cacodylate, pH 7.0.

Crystallization trials were performed by the hanging drop method. Successful crystallization of the HBP–His complex was achieved in two stages. In all stages, the drop was made by mixing 5 μL of protein stock solution and an equal volume of the precipitating solution. The well contained 1 mL of the precipitating solution.

In the initial stage, we used the crystal kit (Hampton Research) for preliminary screening. Only probe no. 6 (0.2 M $MgCl_2$, 0.1 M Tris-HCl, pH 8.5, 30% PEG-4000) yielded crystals which were spherulite or broom-like in shape at cold room temperature and thus unusable. In the second stage, the pH and the types of metal cations in the precipitating solution were varied. The following metal salts at 0.2 M concentration were used: $BaCl_2$, $MgCl_2$, $ZnCl_2$, and $CdCl_2$. The concentration of PEG-8000 in the precipitating solution was kept at 23%. The best crystals were obtained with the precipitating solution of 0.2 M $CdCl_2$, 23% PEG-8000, and 0.05 M Bis-Tris-propane hydrochloride, pH 8.5. These crystals grow to a maximum size of $1.0 \times 0.3 \times 0.1$ mm in 2 days at room temperature.

The crystals, which diffract to at least 1.9-Å resolution, have a $P2_1$ space group with unit cell dimensions of $a = 39.16$ Å, $b = 102.52$ Å, $c = 64.98$ Å, and $\beta = 93.56°$ and volume of 259 700 $Å^3$. Given the molecular weight of 26 000, we find that at only $n = 4$ does the V_m value (the Matthews constant) of 2.49 fall not only within but also very close to the mean of the range. It is thus very likely that the asymmetric unit contains two protein molecules.

Data Collection and Structure Determination. Diffraction intensities to 1.89-Å resolution from one HBP crystals were collected on an SDMS two-detector system mounted on a Rigaku RU200 X-ray generator (Cu Kα radiation) equipped with a graphite crystal monochromator and operated at 110 mA and 40 kV.

The XPLOR suite of programs (Brünger, 1990) was used in the entire structure determination, from molecular replacement to structure refinement. CHAIN (Sack, 1988) was used in the electron density fitting, molecular modeling, and examining of models.

Since the size of the LAOBP and *S. typhimurium* HBP are very similar and their amino acid sequences show approximately 70% identity, we used the known structure of the LAOBP (Kang *et al.*, 1991) as the model in the molecular replacement study. We anticipated initial difficulty in the molecular replacement analysis arising from the fact that the LAOBP structure (coordinates kindly provided by Dr. S.-H. Kim) represents the unliganded "open" form with the two domains far apart and the cleft wide open. On the other hand, the HBP crystals were obtained in the presence of L-histidine and thus are extremely likely to have a structure that conforms to the liganded "closed" form. [After we had determined and refined the HBP structure, a paper describing the structure of the closed form of LAOBP appeared (Oh *et al.*, 1993.] In the closed form seen previously of the structures of several different binding proteins, the two domains engulf and bind the ligand in the cleft between the two domains [for reviews, see Quiocho (1990, 1991)]. Moreover, using the two domains of LAOBP separately as models in the rotational search, no significant rotation peaks were observed.

A successful approach to the molecular replacement procedure was achieved by using an LAOBP structure which was modified on a graphics system so that it mimics the closed liganded structure. The modified model was obtained by (i) breaking the bonds between the Cα and peptide NH of residues 90 and 187 located in the two segments connecting the two domains, (ii) rotating about an axis through the center of the Cα of residue 90 by about 35° in order to bring one domain as close as possible to the other domain without steric clashes, and (iii) reconnecting the two severed bonds. This closed form of the LAOBP model and the intensity data from 8 to 4 Å were used in a cross-rotation search on a 1° grid in modified Eulerian angles θ_+ θ_2 θ_- over the ranges 0–720°, 0–90°, and 0–360°, respectively. The rotational search yielded two strong peaks which were approximately related by a local 2-fold axis ($\psi = -1.8°$, $\phi = 2.7°$, $\kappa = 182.9°$). The top two peaks had rotation function (RF) values of 3.26 and 3.13, respectively, while the highest unrelated peak had an RF of 3.12. Patterson correlation (PC) refinement using a single rigid molecule and the top 72 rotation peaks yielded only two maxima which are extremely similar to those initially found, both with PC values of 0.083 and 0.075. The next highest unrelated peak showed a PC of 0.055.

Using the rotation solutions separately in a one-molecule translation search in the *ac* plane, the top peak for the first search had a correlation coefficient of 0.150 (8σ above the mean) and that for the second search a corresponding value of 0.100 (4σ above the mean). The relative translation along *b* and origin definition were determined in four subsequent translation searches, which differed in the origin shift applied to the second molecule prior to searching with the first molecule. The top correlation coefficients obtained in these searches were 0.138, 0.141, 0.143 (2σ values above the mean), and 0.229 (8σ). These produced an unambiguous result and indicated the correct origin shift of (0, 0, 0.5).

Refinement of the translated LAOBP model at 4-Å resolution with each domain treated as a rigid body reduced

the *R*-factor from an initial value of 0.499 to 0.435. Inspection of the model on the graphics system indicated good crystal packing with no evidence of interpenetration between molecules, especially between the two proteins in the asymmetric unit.

The amino acid sequence of the LAOBP model was changed to that of the *S. typhimirum* HBP (Ames, 1986). The sequence of the *E. coli* HBP is not known. Amino acid analysis of the *E. coli* HBP showed an amino acid composition (with the exception of Asn and Gln residues which were determined as the acidic forms together with the Asp and Glu residues) that is essentially identical to that of the *S. typhimurium* HBP (Trakhanov, 1989; unpublished data). Since amino acid analysis does not distinguish between the acidic residues and their amide counterparts, it would not be possible to detect differences between the sequences of *E. coli* and *S. typhimurium* HBPs due to differences between these isosteric residues. Nevertheless, the number of residues that would be different between the two HBPs must be small, judging from the comparisons of two other pairs of identical binding proteins. The sequences of the sulfate-binding protein from both Gram-negative bacteria are composed of the same number (310) of residues. Both of the sulfate-binding protein sequences differ only in 19 residues, which are conservative and located on the surface of the tertiary structure of the *S. typhimurium* protein and far from the ligand-binding site, the hinge segments connecting the two domains and possible sites for interacting with membrane components of active transport (Jacobson *et al.*, 1991; Pflugrath & Quiocho, 1988; unpublished data). Similar properties are observed in comparing the sequences of the glucose/galactose-binding proteins from *E. coli* and *S. typhimurium*. The glucose/galactose-binding protein sequences from both bacteria, which both consist of 309 residues, differ only in 18 residues. It is therefore not surprising that the crystal structures of the glucose/galactose-binding protein from both sources with bound glucose are extremely similar (Vyas *et al.*, 1988; Mowbray, 1990). On the basis of these comparisons, the differences, if any, between the sequences of the HBPs from both bacteria, which are significantly shorter than those of the four aforementioned binding proteins, will be few and of no consequence to protein function (see below).

A simulated annealing refinement using reflections in the 15–3-Å shell further reduced the *R*-factor to 0.32. Following two cycles of positional and *B*-factor refinements, the *R*-factor was down to 0.24. At this point, the first $(2|F_o| - |F_c|, \alpha_c)$ and $(|F_o| - |F_c|, \alpha_c)$ electron density maps were calculated. These maps were noteworthy and encouraging in the following ways: (1) the $(2|F_o| - |F_c|)$ map was well-defined and the $(|F_o| - |F_c|)$ map generally clear with the exception of a high positive density peak in the center of the molecule; (2) for the most part the refined model of the two HBP molecules fitted the $(2|F_o| - |F_c|)$ density; and (3) clearly present in the center of each protein molecules in both electron density maps, between the two domains, is a well-defined density to which an L-histidine model was fitted easily. Continuing the refinement to convergence at increasing resolutions of 2.4, 2.2, and 1.89 Å, coupled with refitting of the model when necessary and adding ordered water molecules (modeled as oxygens), the final structure was attained. The coordinates of the structure of HBP refined at 1.89 Å have been deposited in the Protein Data Bank.

After completion of the refinement, we carefully and thoroughly scrutinized the residues near the surface of the two independent HBP structures, which have densities [in $(|F_o| - |F_c|)$ maps] that are well-defined or have high quality similar to those of the residues inside the protein molecules, with the intent of identifying the few residues that presumably could be different from the *E. coli* HBP sequence. We could not identify them, however. It is possible that the sequence difference is mostly between isosteric side chains of Asn and Asp and of Gln and Glu which are difficult to distinguish, especially those that are on the surface and not making hydrogen-bonding interactions.

Table 1: Diffraction and Refinement Data of the Histidine-Binding Protein Based on the Structure of Two Molecules in the Asymmetric Unit

data	parameter	value
diffraction	resolution range (Å)	8.0–1.89
	R-sym of 41 075 reflections with no σ cutoff	0.0931
	no. of unique reflections ($F \geq 0\sigma_F$)	28331
	% of theoretical	85
refinement	*R*-factor	0.199
	rms deviation from ideal bond distances (Å)	0.020
	rms deviation from ideal angle (deg)	3.772
	protein atoms	3686
	histidine ligand atoms	22
	cadmium	7
	ordered water molecules	286

RESULTS

HBP Structure. The 1.89-Å refined structure of the histidine-binding protein (two per asymmetric unit) is very good in terms of the quantitative parameters used to judge the correctness of the final model (Table 1). (In keeping with the Protein Data Bank designation, the two independent structures are identified as A and B). The main-chain electron density calculated with $(2|F_o| - |F_c|, \alpha_c)$, contoured at 1σ, is for the most part connected in both A and B proteins. The electron densities of the first three and two residues in molecules A and B, respectively, are not completely resolved.

The entire structure, composed of the A and B HBPs, Cd^{2+} atoms, and ordered solvents (Table 1), has an averaged *B*-factor (Å^2) of 21.5, which is not greatly different from the values calculated for the protein structures alone, the polyglycine backbone, and the side chains. The averaged *B*-factors for only the protein structures are 22.9 for the A protein and 20.1 for the B protein. The values for only the polyglycine backbone are 21.3 and 18.6 for the A and B proteins, respectively, and the side chains are 24.7 and 21.9 for the A and B proteins, respectively.

The HBP structure consists of two globular domains (identified as N- and C-domains or domains 1 and 2, respectively) bisected by a deep cleft, giving it the shape of an ellipsoid with dimensions of approximately 60 × 45 × 40 Å (Figures 1 and 2). The N-domain is folded from two separate peptide segments consisting of residues 1–86 and residues 197–238 from the NH_2- and COOH-termini, respectively. The segment between the two terminal segments (residues 90–192) is allocated to the C-domain, which is only slightly bigger than the N-domain.

The N-domain and C-domain identifications are a carryover from those used previously for several structures of binding proteins with specificities for arabinose/galactose/fucose, glucose/galactose, sulfate, leucine/isoleucine/valine, leucine, and maltodextrins (Quiocho, 1991). These identifications arose from the observation that, in these structures, the NH_2-terminal end is found in the N-domain or domain 1 and the COOH-terminal end in the C-domain or domain 2. Note,

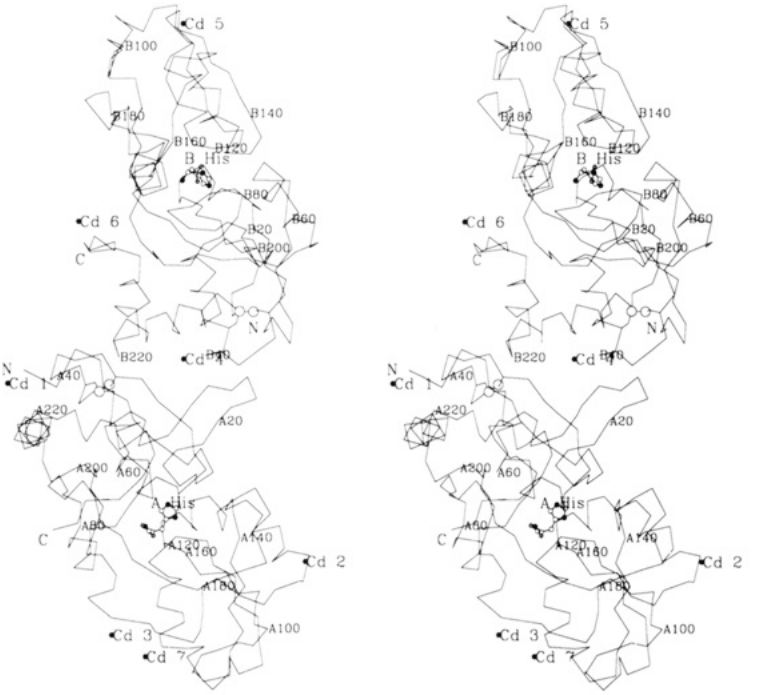

FIGURE 1: Stereoview of the α-carbon backbone traces of the two independent HBP molecules or structures (identified as A, bottom molecule, and B, top molecule) with bound histidine (ball-and-stick model) in the cleft between the two domains. The NH_2- and COOH-terminal ends are labeled with N and C, respectively. Every 20 α-carbons are numbered. Filled circles correspond to the seven Cd^{2+} sites.

FIGURE 2: Stereoview of the ribbon trace of the polypeptide backbone of HBP. The helices are identified by capital Roman numerals and the strands by capital letters (see also Table 2).

however, that both terminal ends of HBP are located in domain 1. This location is similarly observed in the phosphate-binding protein structure (Leucke & Quiocho, 1990), the ribose-binding protein (Mowbray & Cole, 1992), and LAOBP (Kang *et al.*, 1991) (discussed further below). Consequently, domains 1 and 2 are more appropriate and general identifications and will also be used hereafter.

Despite the unequal allocation of the polypeptide segments in the folding of the HBP structure, both domains exhibit similar arrangement of the elements of the secondary structure (Figures 1 and 2). (The elements of the secondary structure are identified in Figure 2, and the segments associated with each element and the domains are listed in Table 2.) Both domains contain a central five-strand β sheet flanked by helices on both sides of the sheet. In domain 1, the β sheet has the topology DAENF in a parallel arrangement with the exception of the N strand which is antiparallel. Two additional short strands (B and C) are associated with domain 1, both forming an antiparallel sheet or a β-ribbon loop which is separate from the main sheet and conspicuously jutting out from the domain structure (Figures 1 and 2). Of the five helices associated with domain 1, two short ones (II and III) abut one side of the sheet and two others which are much longer (I and IX) appose the other side. The fifth, short helix X is alongside helix I. Helices II and III are parallel to each other but oriented opposite to those of the parallel strands. On the other hand, helix I is antiparallel to IX and the sheet.

The five-strand sheet in domain 2 has the topology JIKHL, with H being antiparallel. Although three helices (IV, V, and VIII) are on one side of the plane of the sheet, only helix V is near the sheet running antiparallel to the parallel strands. Helices VI and VII are close to the other side of the sheet.

The segmentation of folding of the polypeptide chain between the two domains naturally gives rise to two hinges (residues 87–89 and 193–196) that connect the domains. Although these interdomain segments are widely separated

Table 2: Secondary Structural Features in the Histidine-Binding Protein

α-helices			strands		
designator	residue segment	domain location[a]	designator	residue segment	domain location[a]
I	28–41	N	A	4–10	N
II	51–61	N	B	17–21	N
III	74–80	N	C	25–28	N
IV	105–110	C	D	44–50	N
V	120–131	C	E	66–69	N
VI	142–153	C	F	81–84	N
VII	161–171	C	G	87–89	N/C
VIII	187–191	C	H	93–97	C
IX	203–220	N	I	112–118	C
X	221–228	N	J	135–140	C
			K	156–161	C
			L	178–181	C
			M	193–196	C/N
			N	197–200	N

[a] N and C refer to the N-domain or domain 1 and the C-domain or domain 2, respectively (see text).

in the sequence, they lie very close to each other in the structure and form a two-stranded (G and M), antiparallel sheet (Figure 2). Strand G originates from strand F in domain I and proceeds to strand H of domain 2. Similarly, strand M of the other hinge bridges strand L of domain 2 with strand N of domain 1.

The two independent A and B HBP structures are very similar. Least squares superimpositioning of the two protein models shows rms deviations of 1.43 Å between the complete models, 0.94 Å between the polypeptide backbones, and 0.93 Å between the α-carbons only (Figure 3). The largest deviations occur in two loops—from residues 181 to 187 and from residues 101 to 107. These are manifested by the 6.5- and 4.9-Å deviations of the α-carbons between residue 183 and between residue 104, respectively. The two loops in both A and B proteins have well-resolved electron density even though they are on the protein surface. The main chains in these loops, with the exception of Gly182 in both proteins, have ϕ, ψ values within the allowable boundaries. The conformations of both loops in the B protein are similar to those of the corresponding loops in the LAOBP structure, which was determined at 2.7-Å resolution. The reason for the conformational differences between the two loops in the A protein and those in the B protein and LAOBP is unclear. The loops in the B protein are close to two symmetry-related A proteins whereas those in the A protein are near only one symmetry-related B molecule. However, the two loops in the A protein are not too distant from the binding site of a cadmium (Cd7)(Figure 1).

Atomic Interaction between HBP and Histidine. The excellent electron density of the ligand-binding sites in the two independent protein molecules, which include the bound L-histidines and nearby residues and water molecules (Figure 4), further attests to the high quality of the refined structure. This quality is further reflected in the *B*-factor averages of 11.2 Å^2 and 13.4 Å^2 for the histidine and the residues responsible for ligand binding (Table 3) in the A and B proteins, respectively. These values are significantly lower than those for the entire refined protein model as indicated above. These features of the ligand-binding sites ensured clear identification of the binding site residues.

Each bound histidine is sequestered in the cleft between the two domains (Figure 1). The atomic interactions between the histidine and HBP in both the A and B structures are extremely similar (Table 3). They are mediated by 10 hydrogen bonds, a couple of salt links, and 63 van der Waals contacts in the A molecule and 61 in the B molecule. The hydrogen-bonding and salt-linking interactions are further highlighted in Figure 4.

A total of 12 residues (7 in domain 1 and 5 in domain 2) are involved in binding the histidine. Interestingly, six of these residues have hydroxyl functional groups (3 Ser, 2 Thr, and 1 Tyr residues) which interact with a total of 11 histidine atoms. As Tyr14 is the single most heavily involved residue in ligand binding, interacting with seven different atoms of the histidine side chain almost exclusively, it plays a dominant role in recognition and binding. Indeed, the aromatic side chain of Tyr14 stacks against the A-face of the histidine ring.

Interestingly, whereas the ammonium and carboxylate groups of the bound histidine make salt links with unpaired charged residues of HBP, the side chain is nowhere near a negatively charged residue (Figure 4 and Table 3). The van der Waals contacts (predominantly with Tyr14) and the three hydrogen bonds (two via two water molecules) are the only means for histidine side-chain recognition. In contrast, model building of the side chains of arginine and lysine in place of that of the histidine indicates that the positively charged side chains could reach and form a salt link with Glu18. (The position of Glu18 is shown in Figure 4.)

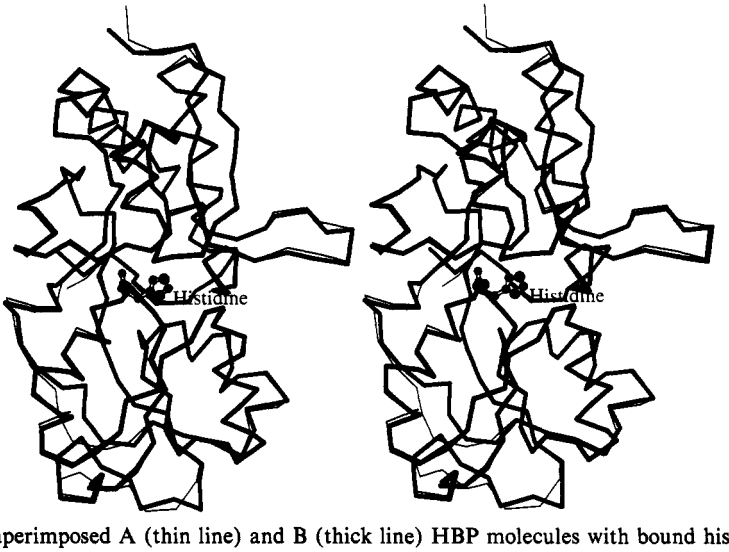

FIGURE 3: Stereoview of the superimposed A (thin line) and B (thick line) HBP molecules with bound histidines.

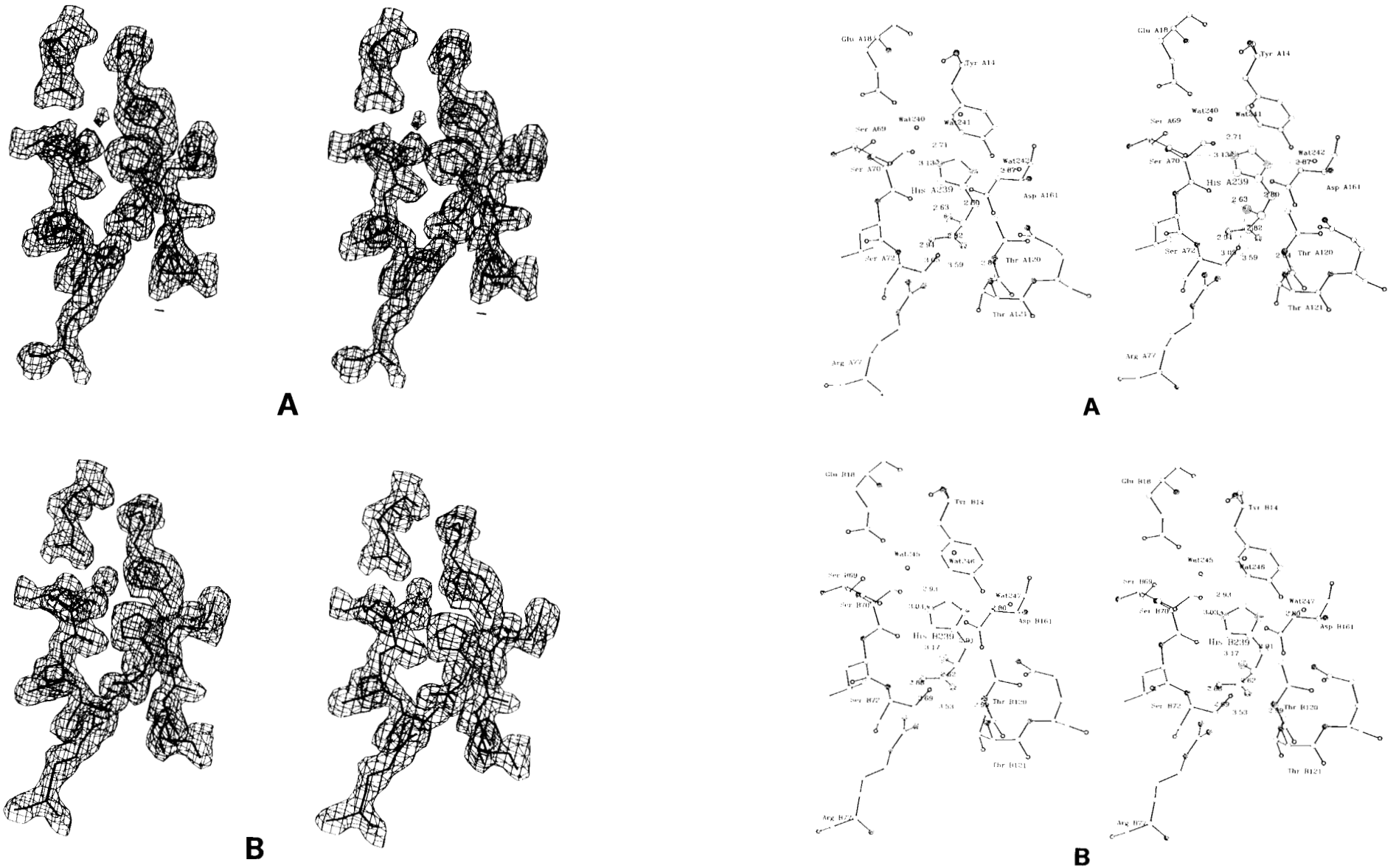

FIGURE 4: Stereo figures of the 1.89-Å ($2|F_o| - |F_c|, \alpha_c$) electron density of the bound histidine and adjacent residues and the hydrogen-bonding interactions (dashed lines) associated with the histidine. The A and B pairs of figures correspond to the A HBP and B HBP structures, respectively. In the electron density maps, calculated with ($2|F_o| - |F_c|, \alpha_c$) after completion of the 1.89-Å structure refinement and contoured at 1σ, the bound histidine is in the center with its side-chain ring apposing the aromatic side chain of Tyr14. Hydrogen bond distances in the models are indicated near the dashed lines. Carbon atoms are depicted as single circles, oxygens as double circles, and nitrogens as triple circles. Hydrogen bonds are shown in dashed lines, and their distances are close to the lines.

Table 3: Contacts between HBP and the Histidine Ligand[a]

histidine atom	residue or water	no. of contact type: A protein	B protein
CA	Ser70	1v	
	Ser72	1v	1v
	Thr121	1v	1v
	Gln122	1v	1v
	Asp161	3v	2v
CB	Tyr14	1v	1v
	Thr120	1v	1v
	Gln122	2v	1v
	Asp161	1v	1v
	Wat242A	1v	
CG	Tyr14	2v	2v
	The120	1v	1v
	Asp161		1v
	Wat242A/247B	1v	1v
CD2	Tyr14	1v	
	Leu52	1v	1v
	Ser69	1v	1v
	Ser70	2v	2v
ND1	Tyr14	3v	4v
	Leu117	1v	
	Thr120	1v	1v
	Wat242A/247B	1h	1h
CE1	Tyr14	4v	6v
	Leu52	1v	1v
	Leu117	1v	1v
	Wat240A/245B	1v	1v
	Wat241A/246B	1v	1v
	Wat242A/247B	1v	1v
NE2	Tyr14	2v	1v
	Leu52	1v	1v
	Ser69	1h	1h
	Wat240A/245B	1h	1h
OT2	Ser70	1v	1v
	Leu71	2v	2v
	Ser72	1h, 2v	1h, 3v
	Arg77[b]	1h, 2v, 1s	1h, 2v, 1s
OT1	Arg77[b]	1h	1h, 2v
	Thr120	4v	4v
	Thr121	1h, 3v	1h, 2v
N	Ser70	1h, 1v	1h
	Ser72	1h, 1v	1h, 2v
	Asp161	1h, 2v, 1s	1h, 2v, 1s
C	Ser72	1v	2v
	Arg77	2v	1v
	Thr121	3v	2v
total		h = 10, v = 63, s = 2	h = 10, v = 61, s = 2

[a] h, hydrogen bond (≤3.5 Å); v, van der Waals contact (≤4 Å); and s, salt link. [b] Although the carboxylate oxygens of the histidine ligand form two distinct hydrogen bonds with Arg77 (Figure 4), these interactions are counted as one salt link.

HBP and LAOBP Structures. As expected, the HBP and LAOBP structures are very similar. Superpositioning of the main chain of domains 1 and 2 of the B HBP structure with domains of the unliganded LAOBP structure gave rms deviations of 0.61 and 1.01 Å, respectively. The residues in the ligand-binding sites of both basic amino acid-binding proteins are almost completely conserved. Only one (Leu52) of the 12 residues of HBP interacting with the histidine (Table 3) is different (Phe residue) in LAOBP (Oh *et al.*, 1993). Leu52 and its Phe counterpart in LAOBP are mainly involved in contacting the side chains, especially the long-chain aliphatic portions, of the amino acids. Asp11 in LAOBP, which makes a salt link with the bound lysine ϵ-ammonium side chain (Oh *et al.*, 1993), is also conserved in HBP, which also binds lysine. Interestingly, Glu18 in HBP (Figure 4), which is within close proximity to Asp11 and is proposed to form a salt link with the ligand lysine side chain (see above), is a Ser residue in LAOBP. Therefore, the side chain of a lysine ligand could potentially form two salt links with Glu18 and Asp11. The substrate specificity between HBP and LAOBP is reflected in differences in one or two residues rather than in several amino acid residues (Higgins & Ames, 1981).

Cadmium Coordinations. We attribute the inclusion of $CdCl_2$ to the crystallization mixture as the sole factor that brought about the ultimate formation of crystals exhibiting superior diffraction. Therefore, it is of interest to know the nature of the interactions associated with Cd^{2+} binding. Seven Cd^{2+} were located in the asymmetric unit (Figure 1), all remote from the histidine-binding site. This is consistent with the finding that histidine-binding activity of the HBP is unaffected by 50 mM Cd^{2+}. The considerable variations in the geometry of the Cd^{2+} coordinations (Figure 5) shed light on this aspect of metal binding as well as on the utility of cadmium in protein crystallization. Since all but one of the bound Cd^{2+} are involved in the interactions betwen proteins in the asymmetric units, they contribute to the formation and stability of the crystal lattice. Cd4 is the only cation bridging the two HBP molecules in the asymmetric unit (Figure 1). Although hexacoordinations dominate the Cd^{2+} binding (Cd sites 2, 4, 5, and 6), they show no common geometry. The remaining cation sites form two pentacoordinations (Cd1 and Cd7) and one tetracoordination (Cd3) which is almost coplanar (Figure 5). With the exception Cd7, all Cd^{2+} are coordinated to carboxylate side chains. Cd2 and Cd4 interact with the greatest number of carboxylate oxygens, a total of four. Cd7 interacts the least with HBP, involving only one histidine side-chain nitrogen. Water molecules are associated with all the bound Cd^{2+}, as much as four with Cd5, Cd6, and Cd7.

DISCUSSION

Overall Structure and Function of Binding Proteins. Including the histidine-binding protein, a total of eight different binding protein structures, respresenting about a third of the entire family of transport receptor proteins from Gram-negative bacteria, have been determined and refined to resolutions of better than 1.9 Å in our laboratory (Quiocho, 1991; unpublished data). The structures determined previously are binding proteins with specificities for arabinose/galactose/fucose, glucose/galactose, maltodextrins (linear and cyclic), leucine/isoleucine/valine, leucine, sulfate, and phosphate (Quiocho, 1992). The glucose/galactose-binding protein and maltodextrin-binding protein (MBP) are also primary components of chemotaxis. All these structures, together with those determined elsewhere such as LAOBP (Oh *et al.*, 1993) and the ribose-binding protein (Mowbray & Cole, 1992), constitute an interesting set for in-depth analysis of protein conformations or domain folding motif and ligand recognition. With the exception of the HBP and LAOBP pair and the leucine/isoleucine/valine-binding protein and leucine-specific binding protein pair which show sequence identities of 70% and 80%, respectively (Higgins & Ames, 1981; Landick & Oxender, 1985; Sack *et al.*, 1989b), the binding proteins with known tertiary structures have little in common with respect to size (M_r ranging from 26 000 for the HBP and LAOBP to 40 000 for the MBP), to amino acid content and sequence, and to specificity for the primary ligands. Nevertheless, these proteins share the following structural features. (1) They have similar overall tertiary structures, consisting of two similar globular lobes separated by a deep cleft. (2) The ligand is bound and sequestered within the cleft. (3) Hinge-bending

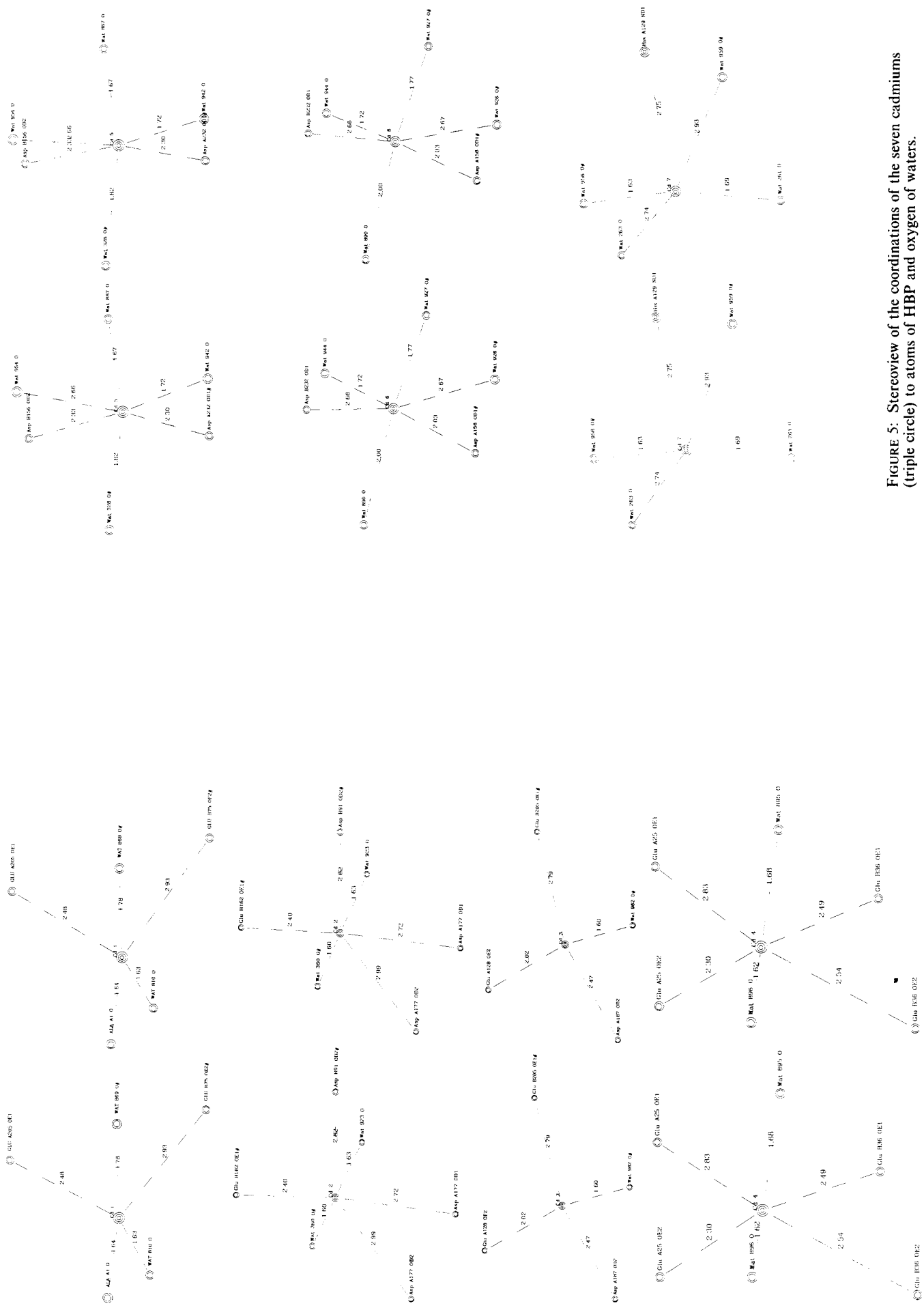

FIGURE 5: Stereoview of the coordinations of the seven cadmiums (triple circle) to atoms of HBP and oxygen of waters.

motion between the two lobes allows access to and from the ligand-binding site. (4) Molecular recognition and binding of the different ligands are achieved principally by hydrogen-bonding interactions.

All these common structural features are in many ways essential for functions. Both domains, in concert with the hinge-bending motion, are used in binding and sequestering the substrate in the cleft and in docking to either of two sets (one for active transport and another for chemotaxis) of proteins components bound in the cytoplasmic membrane. All the structures of the binding protein–ligand complexes show one domain (e.g., domain 1 of HBP) to be more heavily involved in ligand binding than the other domain (Sack *et al.*, 1989a). Docking, using sites on both domains distinct from the ligand-binding site, presumably initiates the processes of active transport and chemotaxis. [The portrayal of the involvement of only a single domain in contacting the membrane components (Higgins & Ames, 1981; Ames, 1986) is inconsistent with the data.]

Functions of Hinge-Bending Motion and the Two Domains. A hinge-bending motion between the two domains has been firmly established as a key feature of binding proteins by a variety of techniques, most clearly by X-ray diffraction in the crystalline state (Sack *et al.*, 1989a; Sharff *et al.*, 1992; Oh *et al.*, 1993; this paper, see Experimental Procedures) and by small-angle X-ray scattering and ^{19}F NMR in solution (Newcomer *et al.*, 1981; Olah *et al.*, 1993; Luck & Falke, 1991). This motion modulates the formations of four structural species—an unliganded open cleft form, an open form with a ligand bound to one domain, an unliganded closed form, and a liganded closed form (Miller *et al.*, 1983; Sack *et al.*, 1989a; Quiocho, 1991). This motion plays at least three crucial roles. It allows easy access to and from the ligand-binding site cleft. It enables both domains to engulf and participate in ligand binding. And it creates a unique distinction, critical in signal transduction in active transport or chemotaxis, between the ligand-bound closed form with the two domains close to each other and the open form with the domains far apart. These roles are best portrayed by two distinct structures of MBP which participates in both transport and chemotaxis—one structure of the unliganded open form and three very similar structures of the closed forms with three different linear maltodextrins bound (Spurlino *et al.*, 1991, 1992; Sharff *et al.*, 1992; L. E. Rodseth, J. C. Spurlino, and F. A. Quiocho, unpublished data). A new finding of the utility of an interdomain rotation is revealed by the binding of a cyclic sugar to MBP. To accommodate the β-cyclodextrin, which is much larger than the linear oligosaccharide substrates, the two domains of MBP remain far apart, very similar to that seen in the unliganded structure, in order to allow the cyclodextrin to be wedged between the two domains (Sharff *et al.*, 1993).

The maltodextrin-binding protein structures, together with very extensive mutational data from the laboratories of Hofnung, Manson, and Shuman (Martineau *et al.*, 1990; Zhang *et al.*, 1992; Hor & Shuman, 1993; and papers cited therein), have also clarified the role of the two domains in the association between a binding protein and membrane-bound components. These studies led to the identification of two sets of several distinct sites on the surface of both domains and the same side of the opening of the cleft, which are used in docking to the two different membrane-bound protein components. One set of sites is involved in binding to the the membrane-bound proteins for active transport and the other group to the chemotactic membrane components. A stringent requirement in the productive docking process, which presumably triggers nutrient translocation or flaggelar motion, is that the membrane components recognize the liganded closed form of the binding protein over the unliganded form. The role of a hinge-bending motion in achieving this requirement, along with promoting full ligand recognition and affinity, is unprecendented.

The β-ribbon loop (residues 17–28; see Figures 1 and 2), which sticks out like a thumb or a peg from domain 1 of HBP close to the opening of the cleft, is also present in the LAOBP structure. It is therefore tantalizing to propose that this loop participates in docking with the transport membrane components. Indeed, this proposal has been previously made following the determination of the structure of LAOBP which also interacts with the same membrane components for histidine transport (Kang *et al.*, 1991; Oh *et al.*, 1993). The strength of this proposal is somewhat diminished by the lack of conservation of the surface residues in the two loops; Glu18, Asn21, and Gln23 in HBP are replaced by Ser, Asp, and Lys, respectively, in LAOBP. On the other hand, the exposed patch formed by Asp114, Ser148, and Arg154 on an α-helix in domain 2 of LAOBP, which is close to the β-ribbon loop in domain 1 and which has been suggested to be involved in contacting the membrane components (Oh *et al.*, 1993), is conserved in HBP.

Dominant Role of Hydrogen Bonds in Ligand Recognition. An unexpected finding from the crystallographic studies is the dominant role that hydrogen bonds play in molecular recognition of the different ligands (Quiocho, 1991). Two features make hydrogen bonds ideal in molecular recognition and binding of ligands. As hydrogen bonds are highly directional, they play a dominant role in conferring specificity on the ligand-binding site. Moreover, a feature which is crucial to active transport is that hydrogen bonds are stable enough to provide the necessary ligand-binding affinities but are of sufficiently low strength to allow rapid ligand dissociation.

Three different examples clearly underscore the importance of hydrogen bonds in molecular recognition. First, as the carbohydrate ligands possess hydroxyl polar functional groups, they are bound mainly by hydrogen bonds. As seen in all of the structures of complexes between binding proteins and carbohydrates (monosaccharides and oligosaccharides), two hydrogen bonds are often associated with each sugar hydroxyl group (Quiocho & Vyas, 1984; Vyas *et al.*, 1988; Spurlino *et al.*, 1991). For example, a total of nine hydrogen bonds are associated with four hydroxyls and the ring oxygen of L-arabinose [see Quiocho and Vyas (1984)]. The arabinose also makes about 55 van der Waals contacts with the protein.

Second, totally unexpectedly, the sulfate dianion that is completely sequestered in the sulfate-binding protein is held tightly in place by seven hydrogen bonds provided solely by uncharged protein donor groups, five peptide backbone NH groups, one OH side chain, and one NH of a Trp side chain (Pflugrath & Quiocho, 1985, 1988). Local dipoles surrounding the sulfate are mainly responsible for stabilizing the uncompensated charges on the oxydianion (Pflugrath & Quiocho, 1985; He & Quiocho, 1993). In a similar mode of binding, the phosphate (either dibasic or monobasic) buried in the cleft of the phosphate-binding protein forms 12 hydrogen bonds with polar groups of the protein which are mostly peptide backbone NHs and hydroxyl side chains (Luecke & Quiocho, 1990). Two of the hydrogen bond donors to the phosphate oxygens are provided by two NH groups of an Arg guanidinium side chain which in turn is paired in a salt link with an Asp carboxylate group. Interestingly, the number of van der Waals

contacts associated with the bound sulfate and phosphate is only about five more than that observed in the arabinose binding.

Third, many hydrogen bonds are also associated with the histidine bound to HBP (Table 3). However, unlike in the binding of the oxyanions to the sulfate- and phosphate-binding proteins, we see for the first time the involvement of salt links with unpaired charged residues in the binding of the amino acid zwitterions lysine to LAOBP (Oh *et al.*, 1993) and histidine to HBP (Figure 4). Indeed, the ammonium side chain of the lysine bound to LAOBP also makes a salt link. These salt links, which presumably possess orders of magnitude greater strength than hydrogen bonds, do not appear to contribute overwhelmingly in the binding affinities of the amino acid zwitterions when compared to affinities seen in binding of arabinose, sulfate, or phosphate.

Two paradoxes emerge from these three examples. First, although the charge content of the four ligands varies (neutral L-arabinose, sulfate and phosphate anions, and histidine and lysine zwitterions), the binding affinities of these ligands are not greatly different—K_ds of 0.098, 0.12, 0.8, 0.03, and 0.015 μM for L-arabinose, sulfate, phosphate, histidine, and lysine, respectively (Miller *et al.*, 1983; Jacobson & Quiocho, 1988; Medvecsky & Rosenberg, 1970; Nikaido & Ames, 1992). Second, although the K_d values are similar, the number and types of hydrogen bonds associated with the ligands vary considerably. The L-arabinose forms five hydrogen bonds with neutral groups and four with charged groups, whereas the phosphate and sulfate make exclusively 12 and 7 charged-neutral hydrogen bonds, respectively. The histidine is engaged in mixed types of hydrogen bonds as well as salt links (Table 3). Presumably, there is a common mechanism that nearly equilizes the strength of ligand affinities despite the differences in the number and types of hydrogen bonds, as well as in the differences in the hydration energies, with charged substrates having significantly greater energies than those of the uncharged sugars. Perhaps this mechanism is related to the conformational change and kinetics of ligand binding (Miller *et al.*, 1983). Undoubtedly, the similarity of ligand affinities, together with the reaction rates, is related to the function of the binding proteins in active transport and chemotaxis (Miller *et al.*, 1983 Luck & Falke, 1991).

Differences between the Binding Protein Structures. Inspite of the four general common structural features that are essential for functions discussed above, there are differences between the 3D structures of the binding proteins. For instance, the binding proteins could be grouped into two, depending on the number of polypeptide segments associated in the folding of each domain. As observed in a greater number of structures, those belonging to group I (binding proteins with specificities for arabinose/galactose/fucose, maltodextrins, glucose/galactose, sulfate, leucine/isoleucine/valine, leucine primarily, and sulfate) are folded from four separate segments (two per domain) of the polypeptide chain. The first (or NH_2-terminal) segment and the third segment (preceding the COOH-terminal segment) constitute the N-domain or domain 1, and the second (following the NH_2-terminal segment) and the fourth or COOH-terminal segments form the C-domain or domain 2. In contrast, the folding of the domains of proteins belonging to group II (such as the phosphate-, histidine-, and ribose-binding protein structures) encompasses only three segments, the NH_2- and COOH-terminal segments making up domain 1 and the one in between the terminal segments being consigned to domain 2. The two groups can be further distinguished as expected by the number of crossovers or hinges between the two domains—three in group I proteins and two in group II proteins. Interestingly, the number of folding segments, hence the number of crossovers between the two lobes, is not strictly related to the size of the proteins. Although the phosphate-binding protein and the sulfate-binding protein are about 1.23 times larges than HBP, the phosphate-binding protein and HBP have three folding segments whereas the sulfate-binding protein has four. However, many more of the larger proteins have four folding segments or three hinges.

We have previously divided the binding protein structures according to the two most prevalent types of transitions or crossovers from one domain to the other (Spurlino *et al.*, 1991), but these types do not strictly follow the two more general groups as distinguished above. The first type of transition is one in which the interdomain segment originates from a β-sheet strand of one domain and terminates into a helix of the other domain. The other type has crossovers originating from and terminating into strands. Whereas the binding proteins with specificities arabinose, glucose/galactose, leucine/isoleucine valine, leucine, and maltodextrins possess mostly the first type of transition, the other binding proteins contain mostly the second type. The multiplicity of interdomain connecting segments restricts the hinge-bending motion to that required for productive ligand binding. Interestingly, the interdomain segment originating from and terminating into helices is less frequently observed.

Finally, although the two domains of the binding proteins have very similar supersecondary structure overall, a central β sheet flanked on both sides by helices, the topological arrangements of the secondary structure elements vary between identical domains [for example, see Spurlino *et al.* (1991)]. This variation is more pronounced between domains 2 than between domains 1. The size difference between the binding proteins is reflected in the variation of the number and length of helices, β-sheet strands, and loops connecting the secondary structure. The size of the binding proteins has no correlation with the specificity for a similar group of ligands. The histidine-binding protein and the leucine/isoleucine/valine-binding protein have molecular weights of 26 100 and 36 700, respectively. The molecular weights of ribose-, arabinose-, and maltodextrin-binding proteins are 29 800, 33 600, and 40 500, respectively. However, most binding proteins have molecular weights of about 35 000 (Furlong, 1987). The two largest proteins bind oligomeric substrates—the maltodextrin-binding protein and the oligopeptide-binding protein ($M_r \approx$ 52 000).

In conclusion, although the histidine-binding protein is one of the smallest of the protein family, its crystal structure resembles overall the other 10 binding protein structures determined previously. The functional features derived from the HBP structure solidify those drawn from the other binding protein structures.

ACKNOWLEDGMENT

We thank Prof. S.-H. Kim for providing the coordinates of the LAOBP without bound ligand in advance of publication.

REFERENCES

Ames, G. F.-L. (1986) *Annu. Rev. Biochem. 55*, 397–425.

Ames, G. F.-L., Mimura, C. S., & Shyamala, V. (1990) *FEMS Microbiol. Rev. 75*, 429–446.

Brünger, A. (1992) *XPLOR3.1: A system for crystallography and NMR*, Yale University, New Haven, CT.

Chang, Z., Choudhary, A., Lathigra, R., & Quiocho, F. A. (1994) *J. Biol. Chem. 269*, 1965–1958.
Furlong, C. E. (1987) in *Escherichia coli and Salmonella typhimurium: Cellular and Molecular Biology* (Neidhardt, F. C., Ingraham, J. L., Low, K. B., Magasanik, B., Schaecher, M., & Umbarger, H. E., Eds.) pp 786–796, American Society for Microbiology, Washington, DC.
Gilson, E., Alliong, G., Schmidt, T., Claverys, J. P., Dudler, R., & Hofnung, M. (1988) *EMBO J. 7*, 3971–3974.
He, J. J., & Quiocho, F. A. (1993) *Protein Sci. 2*, 1643–1647.
Higgins, C. F., & Ames, G. F.-L. (1981) *Proc. Natl. Acad. Sci. U.S.A. 78*, 6038–6042.
Higgins, C. F., Haag, P. D., Nikaido, K., & Ardeshir, F. (1982) *Nature (London) 298*, 723–727.
Hor, L.-I., & Shuman, H. A. (1993) *J. Mol. Biol. 233*, 659–670.
Jacobson, B. L., & Quiocho, F. A. (1987) *J. Mol. Biol. 204*, 783–787.
Kang, C.-H., Kim, S.-H., Nikaido, K., Gokcen, S., & Ames, G. F.-L. (1989) *J. Mol. Biol. 207*, 643–644.
Kang, C.-H., Shin, W.-C., Yamagata, Y., Gokcen, S., Ames, G. F.-L., & Kim, S.-H. (1991) *J. Biol. Chem. 266*, 23893–23899.
Landick, R., & Oxender, D. L. (1985) *J. Biol. Chem.* 260, 8257–8261.
Luck, L. A., & Falke, J. J. (1991) *Biochemistry 30*, 4248–4256.
Luecke, H., & Quiocho, F. A. (1990) *Nature (London) 347*, 402–406.
Macnab, R. (1987) in *Escherichia coli and Salmonella typhimurium: Cellular and Molecular Biology* (Neidhardt, F. C., Ingraham, J. L., Low, K. B., Magasanik, B., Schaecher, M., & Umbarger, H. E., Eds.) pp 732–759, American Society for Microbiology, Washington, DC.
Martineau, P., Saurin, W., Hofnung, M., Spurlino, J. C., & Quiocho, F. A. (1990) *Biochimie 72*, 397–402.
Medveczky, N., & Rosenberg, H. (1970) *Biochim. Biophys. Acta 211*, 158–168.
Miller, D. M., III, Olson, J. S., & Quiocho, F. A. (1980) *J. Biol. Chem. 255*, 2465–2471.
Miller, D. M., III, Olson, J. S., Pflugrath, J. W., & Quiocho, F. A. (1983) *J. Biol. Chem. 258*, 13665–13672.
Mowbray, S. L., & Cole, L. B. (1992) *J. Mol. Biol. 225*, 155–175.
Mowbray, S. L., Smith, R. D., & Cole, L. B. (1990) *Receptor 1*, 41–54.
Nazos, P. M., Su, T. Z., Landick, R., & Oxender, D. L. (1984) *Microbiology* (Leive, L., & Schlessinger, D., Eds.) pp 24–28, American Society for Microbiology, Washington, DC.
Newcomer, M. E., Lewis, B. A., & Quiocho, F. A. (1981) *J. Biol. Chem. 256*, 13218–13222.
Nikaido, K., & Ames, F.-L. (1992) *J. Biol. Chem. 267*, 20706–20712.
Oh, B.-H., Pandit, J., Kang, C.-H., Nikaido, K., Gokeen, S., Ames, G. F.-L., & Kim, S.-H. (1993) *J. Biol. Chem. 268*, 11348–11355.
Olah, G. N., Trakhanov, S., Trewhella, J., & Quiocho, F. A. (1993) *J. Biol. Chem. 268*, 16241–16247.
Pflugrath, J. W., & Quiocho, F. A. (1985) *Nature (London) 314*, 257–260.
Pflugrath, J. W., & Quiocho, F. A. (1988) *J. Mol. Biol. 200*, 163–180.
Quiocho, F. A. (1990) *Philos. Trans. R. Soc. London 326*, 341–351.
Quiocho, F. A. (1991) *Curr. Opin. Struct. Biol. 1*, 922–933.
Quiocho, F. A., & Vyas, N. K. (1984) *Nature (London) 310*, 381–386.
Sack, J. S. (1988) *J. Mol. Graphics 6*, 224–225.
Sack, J. S., Saper, M. A., & Quiocho, F. A. (1989a) *J. Mol. Biol. 206*, 171–191.
Sack, J. S., Trakhanov, S. G., Tsigannik, I. H., & Quiocho, F. A. (1989b) *J. Mol. Biol. 206*, 193–207.
Sharff, A. J., Rodseth, L. E., & Quiocho, F. A. (1992) *Biochemistry 31*, 10657–10663.
Sharff, A. J., Rodseth, L. E., & Quiocho, F. A. (1993) *Biochemistry 32*, 10553–10559.
Spurlino, J. C., Lu, G.-Y., & Quiocho, F. A. (1991) *J. Biol. Chem. 266*, 5202–5219.
Spurlino, J. C., Rodseth, L. E., & Quiocho, F. A. (1992) *J. Mol. Biol. 226*, 15–22.
Trakhanov, S. D. (1989) *Sov. Phys. Crystallogr. 34*, 83–85.
Trakhanov, S. D., Chirgadze, N. Y., & Yusifov, E. F. (1989) *J. Mol. Biol. 207*, 847–849.
Vyas, N. K., Vyas, M. N., & Quiocho, F. A. (1988) *Science 242*, 1290–1295.
Zhang, Y., Conway, C., Rosato, M., Suh, Y., & Manson, M. D. (1992) *J. Biol. Chem. 267*, 22813–22820.